

Spatiotemporal interaction of optical beams in bidispersive media

Nikolaos Moshonas,^{1,*} Yannis Kominis,¹ Panagiotis Papagiannis,¹ Kyriakos Hizanidis,¹ and Demetrios N. Christodoulides²

¹*School of Electrical and Computer Engineering, National Technical University of Athens, 157 73 Athens, Greece*

²*College of Optics/CREOL, University of Central Florida, Orlando, Florida 32816-2700, USA*

*Corresponding author: nmoshon@central.ntua.gr

Received January 12, 2009; revised May 22, 2009; accepted May 24, 2009;
posted May 27, 2009 (Doc. ID 105764); published July 1, 2009

The interaction of optical beams in bidispersive nonlinear media with self-focusing nonlinearity is numerically investigated. Under proper conditions, the interaction of spatially separated beams can lead to the creation of two prominent filaments along the other spatial or temporal dimension and, thus, to an effective spatiotemporal or spatiotemporal exchange. This *X*-wave generation-based effect could potentially be exploited in optical realizations of spatial or spatiotemporal filtering. © 2009 Optical Society of America

OCIS codes: 190.7110, 190.3270, 050.1940, 320.7120, 320.5550, 130.4815.

The propagation of narrow optical beams in media with self-focusing (SF) Kerr nonlinearity has been the focus of intense investigation for many years [1,2]. In the case where two-dimensional (2D) diffraction and anomalous dispersion are present, SF leading to full wave collapse can be observed if the initial power of the beam exceeds a critical value N_c [3]. More recently interest arose in Kerr nonlinear media with normal dispersion where the SF process can be delayed and collapse can be arrested [4–7]. Instead of collapse, pulse splitting may occur along the temporal dimension. This effect is associated with the phenomenon of conical emission. The latter effect is related to the generation and amplification of spectral sidebands that obey a dispersion relation that demands $k_{\perp}^2 \propto \Omega^2$, which represent hyperbolas bound by the cone $|k_{\perp}| = \pm \sqrt{k} \Omega$ (with k being the wavenumber of the beam) [6,8]. This relationship spreads the energy along these “spectral hyperbolas” and strengthens the dispersion factor, which, in turn, redirects the energy away from the center of the wave packet, preventing the collapse and forming two light filaments (one blueshifted and the other redshifted), thus, splitting the beam. We note that these spectral hyperbolas are the same as those involved in spatiotemporal modulational instability (MI), as far as the spectrum of a perturbed continuous wave (CW) is concerned [9]. MI is also responsible for the spontaneous generation of nonlinear *X* waves [10]. Recently, a more involved interpretation was given to this splitting process (or filamentation process, as it is also called) based on “*X*-like” wave packet dynamics [11,12].

These spontaneously generated *X*-shaped light bullets have been observed in lithium triborate $\chi^{(2)}$ crystals [13]. The robust nature of the *X*-like wave packets appearing in cases where normal dispersion is present and their relation with “pulse splitting” has been analyzed in the works of Conti and others [14]. In another recent work, *X*-wave generation was considered by exploiting the inter-

action of a 2D localized Gaussian wave packet and a CW background [15,16]. It was found that the *X*-wave generation process depends on both the relative phase and amplitude of the background with respect to the superimposed wave packet [17,18]. In fact it was the MI of the CW that enabled the creation of these *X*-like structures.

In the present investigation we consider the interaction of two 2D localized wave packets, spatially separated, on top of a broad CW beam. Even though *X*-wave generation is not the aim of this work, the MI generated *X*-like structures are omnipresent. It is thus observed that their interaction can lead to the emergence of two dominant light filaments with temporal separation. In the more general setting of a bidispersive nonlinear medium [16], the temporal dimension is replaced by the other spatial dimension and the aforementioned filaments are now separated spatially, though transversely to the initial (at launching) spatial separation of the beams. The basic idea is illustrated in Fig. 1. Surfaces of constant light intensity in two settings of practical interest are presented, along with a conceptual realization. In Fig. 1(a), two light beams spatially separated at the launching point ($z=0$) end up temporally separated at the end ($z=5$). In Fig. 1(b) it is merely demonstrated that beam interaction does not necessarily allow space–time exchange, i.e., initial temporal separation does not lead to spatial separation. In Fig. 1(c) a possible experimental arrangement is sketched. Two light beams that are simultaneously incident at an angle at two spatially separated ports generate a temporal sequence of two light pulses emanating from the center at the end of the slab waveguide; a weak CW is also injected at the launching point. The current work investigates beam propagation where one transverse spatial and the temporal dimension are considered; thus the terms self-contraction and beam compression, encountered in soliton formation, would be more appropriate than SF, which is used when two spatial dimensions are considered. How-

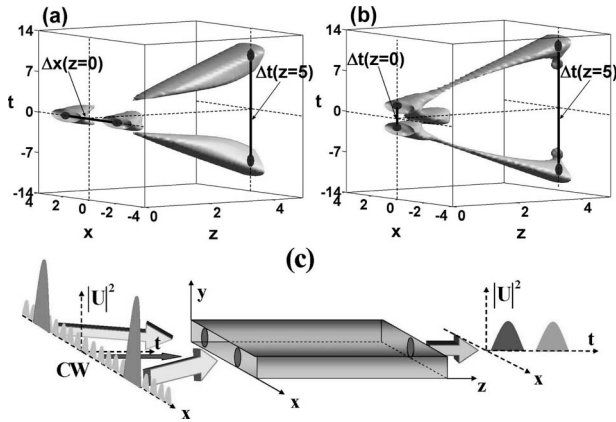


Fig. 1. Isointensity plots at 80% of both the beams intensity. (a) Appearance of two prominent filaments on the temporal axis after the interaction of two spatially localized beams [the same case is also presented in Fig. 4(i)]; (b) two initially temporally localized beams with displacement $\Delta t=4$ lead the output main filaments on the temporal axis; (c) two light beams simultaneously incident at an angle at two spatially separated ports of a conceptual device lead to a temporal sequence of two light pulses emanating from the single center port at the end of the device.

ever due to the analogy of the spatial and temporal terms, which is obvious in Eq. (1), both terms are used.

In the aforementioned configuration (planar normally dispersive waveguide), beam propagation can be described by the following nonlinear Schrödinger equation (NLSE):

$$i \frac{\partial u}{\partial z} + \frac{\partial^2 u}{\partial x^2} - \frac{\partial^2 u}{\partial t^2} + |u|^2 u = 0, \quad (1)$$

where $z=Z/z_0$, $t=(T-Zk')/t_0$, and $x=X/w_0$ are the normalized longitudinal, time, and transverse coordinates, u is the normalized electric field given by $u=E/I_0^{1/2}$, with E being the envelope amplitude and I_0 is the characteristic intensity. As a plausible example, we consider an AlGaAs waveguide operated at $\lambda=1.55 \mu\text{m}$ with a linear refractive index $n=3.34$. The nonlinear coefficient of this system is $n_2=1.5 \times 10^{-13} \text{ cm}^2/\text{W}$ and the normal dispersion parameter is $k''=1.35 \times 10^{-24} \text{ s}^2/\text{m}$. In the examples to follow the beams have a spatial width $w_0=10.5 \mu\text{m}$. Hence $z_0=3 \text{ mm}$, $t_0=45 \text{ fs}$, and $I_0=5.5 \text{ W}/\mu\text{m}^2$. On the other hand, the intensity used for the CW is between 1% and 4% of the maximum beam intensity. The effective horizontal length (x dimension) of the waveguide is not of importance since it is considered very long, its transverse (y dimension) width is taken here to be $1 \mu\text{m}$ and its length is $Z=15 \text{ mm}$ ($z=5$). The relationship of the diffraction and dispersion effects was taken under consideration through the relationship of their respective lengths $L_{\text{df}}=w_0^2 k/2$ and $L_{\text{ds}}=t_0^2/k''$. Their aspect ratio is of major importance and is kept $L_{\text{df}}/L_{\text{ds}}=1/2$ throughout this work.

The evolution of u is greatly affected by its “mass,” defined as $N=\int |u|^2 dx dt$, which in our investigation is actually the “energy” integrated along the transverse spatial and temporal dimensions instead of the power integrated along two spatial dimensions. In this paper we retained the terms “power” and mass, a standard terminology, to point the analogy with previous works. In the case of a single beam propagating in an anomalous dispersive me-

dium, with a power that exceeds a certain critical value, which for Gaussian beams is $N_c=4\pi$, the end result is SF and collapse. Bergé *et al.* [19], in their key work concerning beam interaction, considered the respective initial beam power N_i , in combination with their spatial separation, as a criterion for merging and probable focusing. Here we follow the same guidelines, taking into consideration the role of CW and the features of normal dispersion. On the other hand, SF, which is followed by beam splitting, occurs in media with normal dispersion, for powers that are usually greater than N_c , and is related to the aspect ratio of the diffraction and dispersion lengths [5]. Since here we assume the coexistence of two localized Gaussian beams along with a CW background, we can consider u as a superposition of beams u_1 and u_2 with u_{CW} , namely, $u=u_1+u_2+u_{\text{CW}}$. It is assumed that the mass variation, ΔN_i , generated by the interaction of the beams with the CW is incorporated in the individual beams themselves. This assumption can be easily met if one considers that the CW, or quasi-CW, beam is of low intensity but of infinite (or very large) energy, thus effectively constant. Hence, one may set $u=u_1+u_2+u_{\text{CW}}$, where

$$u_{1,2} = A \exp \left[-\frac{(x \mp x_0)^2 + (t - t_0)^2}{2} \pm i \Delta k_x x + i \phi_{1,2} \right],$$

$$u_{\text{CW}} = A a_{\text{CW}} \exp(-i\varphi), \quad (2)$$

where A is the amplitude of the beams, $\Delta x=2x_0$ and $\Delta t=2t_0$ are the initial spatial and temporal wave packet separations, Δk_x is the initial transverse wavenumber mismatch, ϕ_1 and ϕ_2 are the initial phases of the beams, a_{CW} is the relative amplitude of the CW, and φ is its phase. Spatiotemporal integration of the total mass $|u_{1,2}+u_{\text{CW}}|^2$ yields the individual finite modified masses,

$$N_i + \Delta N_i = N_i [1 + 4a_{\text{CW}} \cos(\Delta\phi_i + \Delta k_x \Delta x/2) \exp(-|\Delta k_x|^2/2)], \quad (3)$$

where $\Delta\phi_i = \phi_i - \varphi$ ($i=1, 2$) is the phase difference of the respective beam with the CW. This, in turn, should change the individual beam power necessary for compression and splitting and can also affect the process of merging and the probable SF thereafter. According to [5], for the value of the aspect ratio between the diffraction and dispersion lengths, considered here, the necessary power that can trigger individual SF, and consequent splitting, of a wave packet is not N_c but more than $2N_c$. We use this result as a point of reference for our case of study and actually observe a similar response. The interaction of the beams depends not only on their relative phase but also on the individual powers [18,19]. It is well known that, in general, in-phase beams undergo mutual attraction, π , out of phase repel each other, while for intermediate values of phase difference beams can experience inelastic collisions [20]. The numerical investigation that follows takes into consideration all of the above.

In Figs. 2–4 the horizontal axis corresponds to the spatial (x) dimension and has a length of 50 transverse pulse widths (-263 to $263 \mu\text{m}$) and the vertical axis corresponds to the temporal (t) dimension at a length of 50 pulse widths (-1.12 to 1.12 ps). The color bars are placed for in-

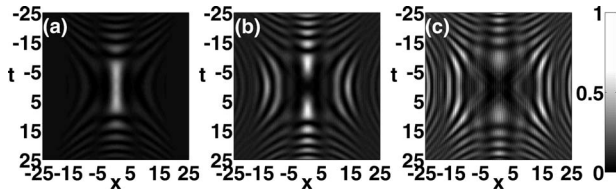


Fig. 2. Output intensity profile at $z=5$ (15 mm), with $a_{CW}=0.1$, $\varphi_1=\varphi_2$, $\varphi=0$, and $\Delta x=4$. The input power was initially set at (a) $N_i=0.9N_c$, (b) $N_i=1.85N_c$, and (c) $N_i=3N_c$.

tensity comparison. A picture of the initial beam placement along x can be provided by Fig. 1(a) at $z=0$.

The NLSE is solved via a beam propagation method. In all cases the spatiotemporal window is taken broad enough to avoid artificial reflections from the boundaries. The CW is retained throughout this investigation since its presence retards the diffraction of the beams and helps the concentration of the energy in relation to the MI created structures [15]. Furthermore, without any loss of generality we also set $\varphi_1=\varphi_2$. In Fig. 2, the output intensity profiles are shown at $z=5$ (at 15 mm) when two beams are launched simultaneously, with $\Delta x=4$ (42 μm for the reference example), $\Delta\phi_i=0$, $\Delta k_x=0$, and in the presence of a CW with $a_{CW}=0.1$. The initial beam powers are varying, and in Fig. 2(a) $N_i=0.9N_c$, which, even with ΔN_i added, is lower than the minimum needed power for the beams to merge and focus [19]. That should not happen no matter how close the two beams might start. In this case, the beams diffract, but the energy is weakly concentrated in a low central lobe and along hyperbolic curves, resembling an X-like structure. For beams with $N_i=1.85N_c$ [Fig. 2(b)], their power is high enough that along with the part offered by the CW force them to start individual splitting. Nevertheless, soon after this splitting starts, the filaments merge along the temporal axis. However, the energy is not concentrated in two prominent lobes but in many smaller ones. For an even higher beam power ($N_i=3N_c$), the result is multiple splitting and filamentation [Fig. 2(c)].

Next we investigate the effect of initial spatial separation of the beams. Beam power is set at $N_i=1.5N_c$ and the CW is of higher amplitude than before, namely, $a_{CW}=0.2$. Thus, the power that can trigger individual compression and splitting is also expected to be close to $1.5N_c$. For $\Delta x=3$, in Fig. 3(a), the two beams tend to temporally split, but they soon merge. Two individual filaments of opposite frequency sidebands emerge and draw away from each other, but many other smaller peaks appear. For $\Delta x=4$, the beams split individually, but the filaments merge and concentrate at the t -intercept points of the first hyperbola. This is a more favorable result, since these filaments have

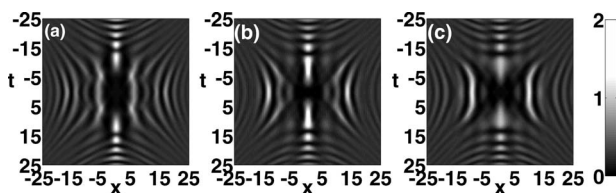


Fig. 3. Output intensity profile at $z=5$ (15 mm) for initial spatial separations: (a) $\Delta x=3$, (b) $\Delta x=4$, (c) $\Delta x=5$. In all cases, $a_{CW}=0.2$, $\varphi_1=\varphi_2$, $\varphi=0$, and $N_i=1.5N_c$.

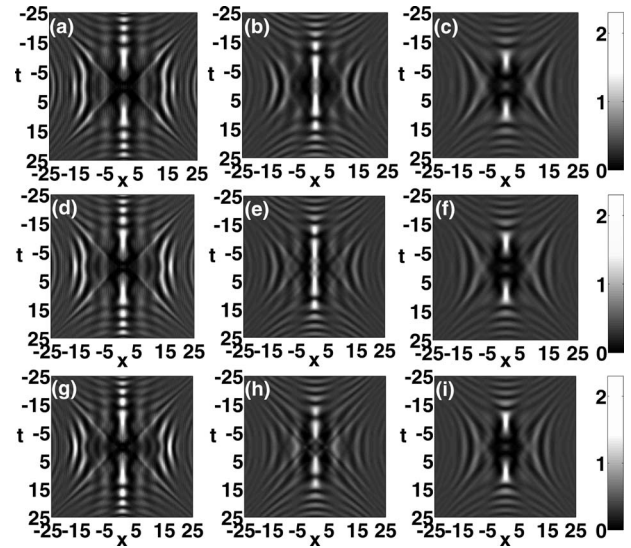


Fig. 4. Output intensity profile, at $z=5$, in the presence of a CW, with $a_{CW}=0.2$, for various values of its phase (φ) and for various values of the wave packets initial transverse wavenumber difference (Δk_x); (a),(d),(g) $\varphi=0$, (b),(e),(h) $\varphi=\pi/2$, (c),(f),(i) $\varphi=\pi$; (a),(b),(c) $\Delta k_x=0$, (d),(e),(f) $\Delta k_x=0.1$, (g),(h),(i) $\Delta k_x=0.2$. In all cases, initial values were set to $N_i=2N_c$, $\Delta x=4$, and $\varphi_1=\varphi_2$.

significantly more power than the rest that are being created, but they emerge rather late, around $z=4$. They move away along the t axis and retain their amplitude until $z=5$. For $\Delta x=5$ we observe individual splitting, as it has been expected considering the amount of the individual masses. Diffraction spreads the energy, mainly along the x -centered hyperbolas.

We next consider how the spatial wavenumber mismatch between the beams and their phase difference with the CW affect the beam evolution. The relative phase between the beams is set to zero, $a_{CW}=0.2$, $\Delta x=4$, and $N_i=2N_c$. Figure 4 presents the output profiles for $\Delta k_x=0$ [Figs. 4(a)–4(c)], 0.1 [Figs. 4(d)–4(f)], and 0.2 [Figs. 4(g)–4(i)] and $\varphi=0$ [Figs. 4(a)–4(g)], $\pi/2$ [Figs. 4(b)–4(h)], and π [Figs. 4(c)–4(i)]. For $\varphi=0$, the CW adds a lot of energy to the beams resulting in individual splitting along time and generation of many small lobes of nearly equal amplitude. The higher the wavenumber mismatch, the more “momentum” the initial beams have and the more obvious the merging and multiple filamentation are [Figs. 4(a)–4(g)]. For $\varphi=\pi/2$, the CW does not add any amount of energy to the beams, at least initially. The beams do not self-contract, the initial power is not enough for this to happen. Instead, they disperse but finally merge at the center and split twice. Four filaments are formed, of relatively equal amplitude, which they retain. The case of $\varphi=\pi$ gives the most efficient intensity reallocation [Figs. 4(c)–4(i)]. In this case the CW takes away power from the initial beams. Also, the less their relative wavenumber mismatch is, the more power is “subtracted” from them. The beams disperse quickly, moving to create two filaments of their own along the temporal axis, but then they finally merge in one central lobe that splits in two other lobes (around $z=2.5$) with their peaks positioned at $x=0$ and moving along time, thus emerging at $z=5$ clearly separated in time. Although convergence of the beams ($\Delta k_x>0$) does not affect the outcome strongly, even better

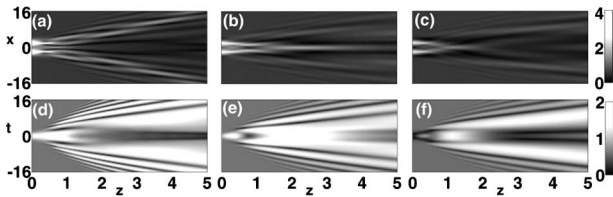


Fig. 5. (a)–(c) Spatial and (d)–(f) temporal intensity profiles during propagation for $\Delta k_x=0.2$, $a_{CW}=0.2$, $N_i=2N_c$, $\varphi_1=\varphi_2$, $\Delta x=4$, and (a),(d) $\varphi=0$, (b),(e) $\varphi=\pi/2$, (c),(f) $\varphi=\pi$.

results are attained for slightly converging beams [Figs. 4(f) and 4(i)]. In the latter case of $\Delta k_x=0.2$ the resulting main filaments possess higher peak intensity than of $\Delta k_x=0.1$ (1.5 versus 1.3). In Fig. 1(a) the latter, more favorable, case is shown. An initial spatial separation $\Delta x=4$ (42 μm for the reference example) leads to a temporal separation $\Delta t=16$ (0.7 ps for the reference example). Furthermore, in Fig. 5 the spatial [Figs. 5(a)–5(c)] as well as the temporal [Figs. 5(d)–5(f)] evolution is shown for the respective Figs. 4(g)–4(i) cases. What is also obvious from the previous figures is that the energy, either concentrated in prominent filaments or more dispersed along hyperbolic formations, tends to be localized on certain hyperbolas, as analyzed in [21].

In Fig. 6 the movement, along the t dimension of the highest emerging filaments is presented by tracking the peak power of the bottom filament (the one moving along the “negative” time, meaning the slower of the two). The z axis of propagation is presented for $z \geq 2$, where the formation of the time separated filaments has been concluded. The cases of $\varphi=0$ with $\Delta k_x=0$ and 0.1 (thick and thin full curves, respectively), $\varphi=\pi/2$ with $\Delta k_x=0.2$ (dashed curve) and $\varphi=\pi$ with $\Delta k_x=0$ and 0.2 (thick and thin dotted curves, respectively) are presented. It seems that small values of the wavenumber mismatch do not affect the temporal displacement of the major emerging filaments considerably. On the other hand, the phase difference between the beam and the CW does affect the distance where these filaments emerge, as well as their spectral content (in the case of $\varphi=0$ the filaments move apart faster than in the case of $\varphi=\pi$). What cannot be shown in Fig. 6, but is more obvious in Fig. 4, is that for the $\varphi=0$ case secondary peaks are born that are of intensity almost equal to the intensity of the major emerging

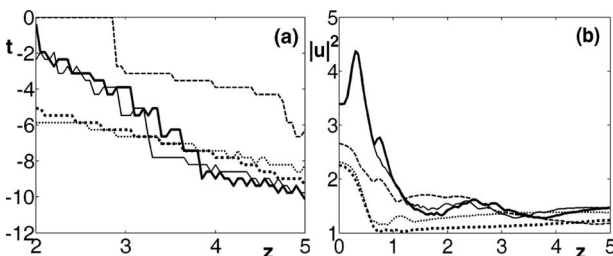


Fig. 6. (a) Movement of one of the two major filaments after the splitting and their clear emergence for various cases of initial wavenumber mismatch and CW phase values. Horizontal axis depicts the normalized propagation distance and vertical axis is the normalized time. Thick and thin full curves represent the cases of Figs. 4(a) and 4(d), thick and thin dotted curves represent the cases of Figs. 4(c) and 4(i), and the dashed curve represents the case of Fig. 4(h), respectively. (b) Peak intensity evolution for the same cases.

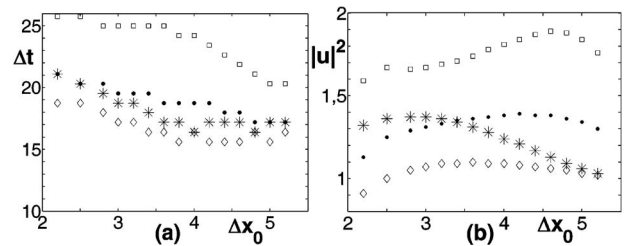


Fig. 7. Numerical investigation of (a) the output temporal displacement of the two prominent filaments versus initial spatial separation (Δx_0) and (b) their respective intensity, for various values of the initial individual beam mass (diamonds, $N=1.5N_c$; stars and black dots $N=2N_c$; squares $N=3N_c$), while $a_{CW}=0.2$, $\varphi=\pi$, and $\Delta k_x=0.2$, except for the stars where $\Delta k_x=0$.

filaments. In the $\varphi=\pi/2$ case the filaments appear a bit “slower” than in the other cases. In fact the energy of the merging beams stays within the central lobe for a greater propagation distance than at the other cases, before it splits. In Fig. 6(b), the maximum intensity of the major emerging filaments is presented, for the cases of Fig. 6(a). It is shown that in all cases the major emerging filaments have almost equal peak intensity, which they retain, at least until $z=5$.

A comparison of the temporal displacement between the two main output filaments and between their peak intensities can be viewed in Figs. 7(a) and 7(b). For all the cases $a_{CW}=0.2$ and $\varphi=\pi$, while $\Delta k_x=0.2$ is the standard for most of the calculations. It seems that the initial spatial displacement (either small or larger and the subsequent quick merging or individual splitting for higher powers) does affect the output ($z=5$) temporal displacement but not dramatically. Its influence is larger for high initial input power. The initial power itself seems to be an important factor and the greater it is, the higher is the intensity of the filaments and the greater their displacement. A comparison of the two cases for $N=2N_c$ indicates that a nonzero initial beam convergence in combination with a very small initial spatial separation leads not only to a quick merging but also to a wider dispersion of the energy and output filaments of low intensity. However, for larger spatial separations a small initial convergence helps energy concentration and finally leads to a larger temporal displacement and higher intensity of the output filaments. For even higher powers the result is multiple splitting with no prominent filaments.

One-dimensional Fourier transform of the temporal dimension has also been conducted for $z=0$ and $z=5$ for the case of Fig. 4(i) [Figs. 8(a) and 8(b)]. In Fig. 8(b) we can see that there are energy concentrations at opposite frequency bands, symmetrically placed above and below the initial beam frequency, which is zero in normalized values. Being placed at $x=0$, their opposite frequencies/velocities represent the opposite and increasing temporal displacement of the output filaments. The white horizontal line shown in Figs. 8(a) and 8(b) represents the monochromatic CW.

In conclusion, it has been shown that the interaction between two spatially separated localized wave packets and a CW background can lead to the creation of two temporally distinct filaments. The propagation distance where the filaments emerge, as well as their initial posi-

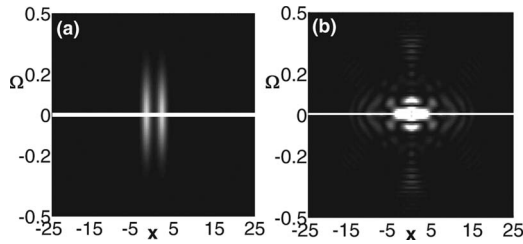


Fig. 8. Frequency displacement Ω versus spatial dimension for the input ($z=0$) and output ($z=5$) at (a) and (b), respectively. The horizontal axis always represents the spatial (x) dimension and is measured in w_0 . The vertical axis is the frequency displacement and is in normalized units $\Omega_0=2\pi/t_0=140$ THz. The white line represents the CW.

tion on the time axis, their intensity, and robustness depend on the initial characteristics of the interacting beams, as well on these of the CW. The above observations indicate that a controllable all-optical spatial or spatiotemporal switching and filtering are possible in such systems.

REFERENCES

- J. J. Rasmussen and K. Rypdal, "Blow-up in nonlinear Schrödinger equations. I. A general review," *Phys. Scr.* **33**, 481–497 (1986).
- L. Bergé, "Wave collapse in physics: principles and applications to light and plasma waves," *Phys. Rep.* **303**, 259–370 (1998).
- Y. Kivshar and D. E. Pelinovsky, "Self-focusing and transverse instabilities of solitary waves," *Phys. Rep.* **331**, 117–194 (2000).
- P. Chernev and V. Petrov, "Self-focusing of light pulses in the presence of normal group-velocity dispersion," *Opt. Lett.* **17**, 172–174 (1992).
- G. G. Luther, J. V. Moloney, and A. C. Newell, "Self-focusing threshold in normally dispersive media," *Opt. Lett.* **19**, 862–864 (1994).
- G. G. Luther, J. V. Moloney, A. C. Newell, and E. M. Wright, "Short-pulse conical emission and spectral broadening in normally dispersive media," *Opt. Lett.* **19**, 789–791 (1994).
- J. K. Ranka, R. W. Schirmer, and A. L. Gaeta, "Observation of pulse splitting in nonlinear dispersive media," *Phys. Rev. Lett.* **77**, 3783–3786 (1996).
- A. G. Litvak, V. A. Mironov, and E. M. Sher, "Regime of wave-packet self-action with normal dispersion of the group velocity," *Phys. Rev. E* **61**, 891–893 (2000).
- L. W. Liou, X. D. Cao, C. J. McKinstrie, and G. P. Agrawal, "Spatiotemporal instabilities in dispersive nonlinear media," *Phys. Rev. A* **46**, 4202–4208 (1992).
- C. Conti, "X-wave mediated instability of plane waves in Kerr media," *Phys. Rev. E* **68**, 016606 (2003).
- M. Kolesik, E. M. Wright, and J. V. Moloney, "Dynamic nonlinear X waves for femtosecond pulse propagation in water," *Phys. Rev. Lett.* **92**, 253901 (2004).
- D. Faccio, M. A. Porras, A. Dubietis, F. Bragheri, A. Couairon, and P. Di Trapani, "Conical emission, pulse splitting and X-wave parametric amplification in nonlinear dynamics of ultrashort light pulses," *Phys. Rev. Lett.* **96**, 193901 (2006).
- P. Di Trapani, G. Valiulis, A. Piskarkas, O. Jedrkiewicz, J. Trull, C. Conti, and S. Trillo, "Spontaneously generated X-shaped light bullets," *Phys. Rev. Lett.* **91**, 093904 (2003).
- C. Conti, "Generation and nonlinear dynamics of X waves of the Schrödinger equation," *Phys. Rev. E* **70**, 046613 (2004).
- Y. Kominis, N. Moshonas, P. Papagiannis, K. Hizanidis, and D. N. Christodoulides, "Continuous wave controlled nonlinear X-wave generation," *Opt. Lett.* **30**, 2924–2926 (2005).
- D. N. Christodoulides, N. K. Efremidis, P. Di Trapani, and B. A. Malomed, "Bessel X waves in two- and three-dimensional bidispersive optical systems," *Opt. Lett.* **29**, 1446–1448 (2004).
- N. N. Akhmediev and S. Wabnitz, "Phase detecting of solitons by mixing with continuous wave background in an optical fiber," *J. Opt. Soc. Am. B* **9**, 236–242 (1992).
- Y. Kominis and K. Hizanidis, "Solitary wave interactions with continuous waves," *Int. J. Bifurcation Chaos Appl. Sci. Eng.* **16**, 1753–1764 (2006).
- L. Bergé, M. R. Schmidt, J. J. Rasmussen, P. L. Christiansen, and K. Ø. Rasmussen, "Amalgamation of interacting light beamlets in Kerr-type media," *J. Opt. Soc. Am. B* **14**, 2550–2562 (1997).
- G. I. Stegeman and M. Segev, "Optical spatial solitons and their interactions: universality and diversity," *Science* **286**, 1518–1523 (1999).
- L. Bergé, K. Germaschewski, R. Grauer, and J. J. Rasmussen, "Hyperbolic shock waves of the optical self-focusing with normal group-velocity dispersion," *Phys. Rev. Lett.* **89**, 153902 (2002).